Biophysical Chemistry 159 (2011) 227–236

Contents lists available at ScienceDirect

Biophysical Chemistry

journal homepage: http://www.elsevier.com/locate/biophyschem

Theoretical study of the excited states of the photosynthetic reaction center in photosystem II: Electronic structure, interactions, and their origin

Yuya Kitagawa [a], Kenji Matsuda [a], Jun-ya Hasegawa [a,b,*]

[a] Department of Synthetic Chemistry and Biological Chemistry, Graduate School of Engineering, Kyoto University, Nishikyo-ku, Kyoto 615-8510, Japan
[b] Quantum Chemistry Research Institute (QCRI) and JST-CREST, Kyodai Katsura Venture Plaza, Goryou Oohara 1-36, Nishikyo-ku, Kyoto 615-8245, Japan

ARTICLE INFO

Article history:
Received 26 February 2011
Received in revised form 17 June 2011
Accepted 17 June 2011
Available online 3 July 2011

Keywords:
Photosystem II
Reaction center
Ab initio excited-state calculation
Absorption spectrum
Molecular interaction
Charge-transfer state

ABSTRACT

The excited states of the chlorophyll 6-mer in the photosystem II (PSII) reaction center (RC) were investigated theoretically using ab initio quantum chemical calculations, and the results are compared with those of the bacterial reaction center (bRC). A significant difference in the peak at the lowest energy in the absorption spectra arises from the structural asymmetry of the special pair (SP). The origin can be traced back to the structural difference in the CD helix. The low-lying excited states are characterized as a linear combination of the excited states of the chlorophyll monomers, which verifies the applicability of exciton theory. Analysis of the molecular interactions clearly explains the cause of the constructive/destructive interferences in the state transition moment. The protein electrostatic potential (ESP) decreases the energy of the charge-transfer ($Chl_{D1} \rightarrow Pheo_{D1}$) state. The ESP also localizes the HOMO distribution to the P_{D1} moiety and increases the ionization potential.

1. Introduction

Photosystem II (PSII) is found in the thylakoid membrane of plants and cyanobacteria [1,2] and produces molecular oxygen using solar energy as a source of energy [1,2]. As shown in Fig. 1a, the photosynthetic reaction center (RC) in PSII contains chlorophyll (Chl) and pheophytin (Pheo) compounds: P_{D1}, P_{D2}, Chl_{D1}, Chl_{D2}, $Pheo_{D1}$, and $Pheo_{D2}$ [3]. The subscripts D1 and D2 indicate that the chlorophylls are involved in the D1 and D2 subunits of the RC protein, respectively. P_{D1} and P_{D2} lie close to each other and are called special pair (SP). Photochemistry in the PSII RC starts with electron excitation in one of the chromophores in the light-harvesting system [1,2]. The excitation is transferred to the RC and is used for electron transfer across a thylakoid membrane [1,2,4].

Because the PSII RC [5] shares evolutionary origins with the purple bacterial RC (bRC) [6,7], the structures of the two RCs are very similar. Regarding the electron transfer, the two RCs show similar pathway selectivity. The electron transfer in PSII [8,9] RC and bRC [10] occurs only along the D1 branch (which is called the "L branch" in bRC). However, regardless of their structural similarities, the absorption spectra of the two RCs are very different as shown in Fig. 2. In the case of bRC, the lowest absorption peak originates from the first excited state of SP and shows a characteristic red-shift compared with the other chlorophylls [10]. In contrast, no such spectral shift is observed in the case of the PSII RC [11,12], indicating that the molecular interactions among the excited Chls are different.

To understand the excited states, photoabsorption spectrum, and energy transfer of PSII, theoretical calculations using the excitonic coupling have been performed [13–18] using X-ray crystal structures [13,19]. In a multimer model, the excited states are considered to be delocalized among the chromophores [14,15,20]. In contrast, a photon-echo study [12] proposed that the Chl_{D1} monomer is the primary donor, which is supported by recent theoretical investigations [17,18].

Although previous studies [16–18,21] recognized that the molecular interactions between the chromophores define the character and function of the excited RCs, there has been no quantum chemical calculation in which the excited states of the RC were calculated at the ab initio level. Because the intermolecular distances between neighboring chromophores are approximately 3 Å, it is not clear if the Förster dipole approximation to the Coulomb interaction can reproduce the results with the original Hamiltonian. Quantum chemical calculations were performed to evaluate excitonic coupling between the chromophores [16,22,23]. In the case of the PSII RC, the results of the dipole approximation was compared with that obtained with transition charges from electrostatic potential (TrEsp) [24] method [18]. In the case of photosystem I, the result of the dipole approximation was compared [22] with those evaluated using a quantum mechanical method [25]. These studies showed that the dipole approximation overestimates the electronic coupling in the SP [18] and underestimates the coupling between the SP and accessory chlorophylls [22], indicating the importance of quantum mechanical

* Corresponding author at: Department of Synthetic Chemistry and Biological Chemistry, Graduate School of Engineering, Kyoto University, Nishikyo-ku, Kyoto 615-8510, Japan. Tel.: +81 75 383 2746; fax: +81 75 383 2741.
E-mail address: hasegawa@sbchem.kyoto-u.ac.jp (J. Hasegawa).

0301-4622/$ – see front matter © 2011 Elsevier B.V. All rights reserved.
doi:10.1016/j.bpc.2011.06.011

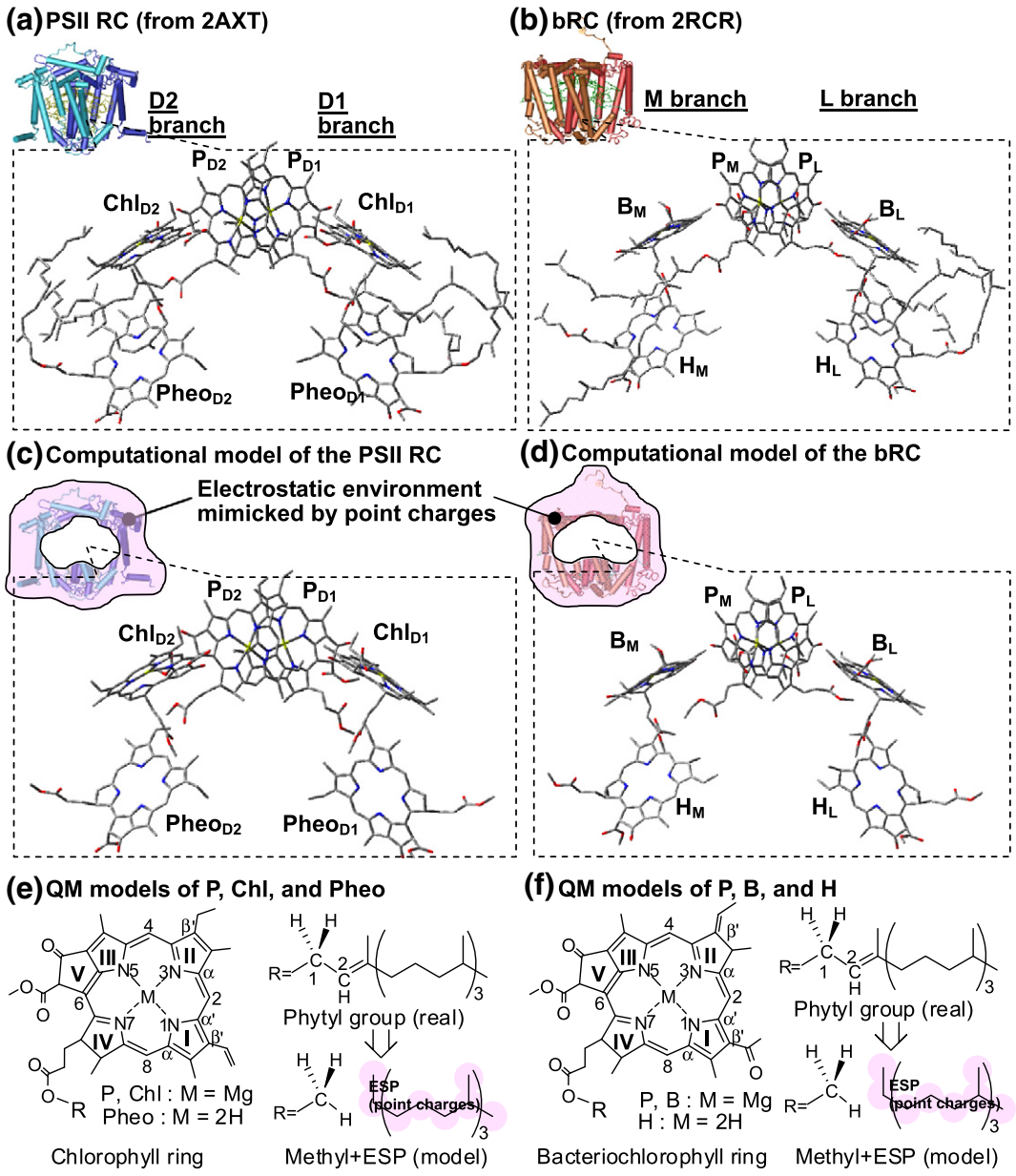

Fig. 1. X-ray structures of the chlorophyll hexamer involved in (a) the PSII RC [3] and (b) the bRC [27]. Computational models of the hexamers for (c) the PSII RC and (d) bRC. Hydrogen atoms were omitted for clarity. Electrostatic potential from protein environments (colored pink) were described by point-charge models. Structures of (e) chlorophyll *a* and pheophytin *a* in the PSII RC and (f) structures of bacteriochlorophyll *b* and pheophytin *b* in the bRC, and their computational models. The electrostatic potential from the phytyl group (colored pink) was described by a point-charge model.

effects in short-range interactions [23]. The ionized potential of the SP in the PSII RC was calculated at the DFT level [26]. The HOMO distribution was found to be delocalized over the two chlorophyll monomers [26]. The results might indicate the limit of the applicability of exciton theory to the excited states of the PSII RC, which should be examined by quantum chemical calculations for the excited states of the RC.

In this study, we performed ab initio CI-Singles (CIS) calculations to investigate the excited states of PSII RC, and the result is compared with that of the bRC. First, we discuss the absorption spectrum and attempt to explain why no significant red-shift occurs in the lowest absorption peak of the PSII RC. The origin of the difference between PSII RC and bRC is investigated in terms of the molecular orientation, orbital interactions, and protein structure. The electronic structures of the excited states were analyzed, and the applicability of the exciton theory has been verified. To characterize the molecular interactions underlying the spectrum shape, we introduce a diagram that explains the magnitude of the transition dipole moment (TDM) of the excited states. We also mention the effect of the protein electrostatic potential (ESP) on the excitation energies, particularly for charge-transfer (CT) states, and also on the ionization potential.

2. Computational details

The present computational models were based on X-ray structures, 2AXT [3] and 2PRC [27] for PSII RC and bRC, respectively. Because of the difficulties in the geometry optimization of the chromophore aggregate in the protein, we used the X-ray structures for most of the atoms. We note, however, that there is a pioneering work of Reimers and co-workers in which the structure of PSI was quantum mechanically optimized [28]. Instead, we investigated the bond lengths of the chromophores in the X-ray data and found that the bond lengths are close to those calculated

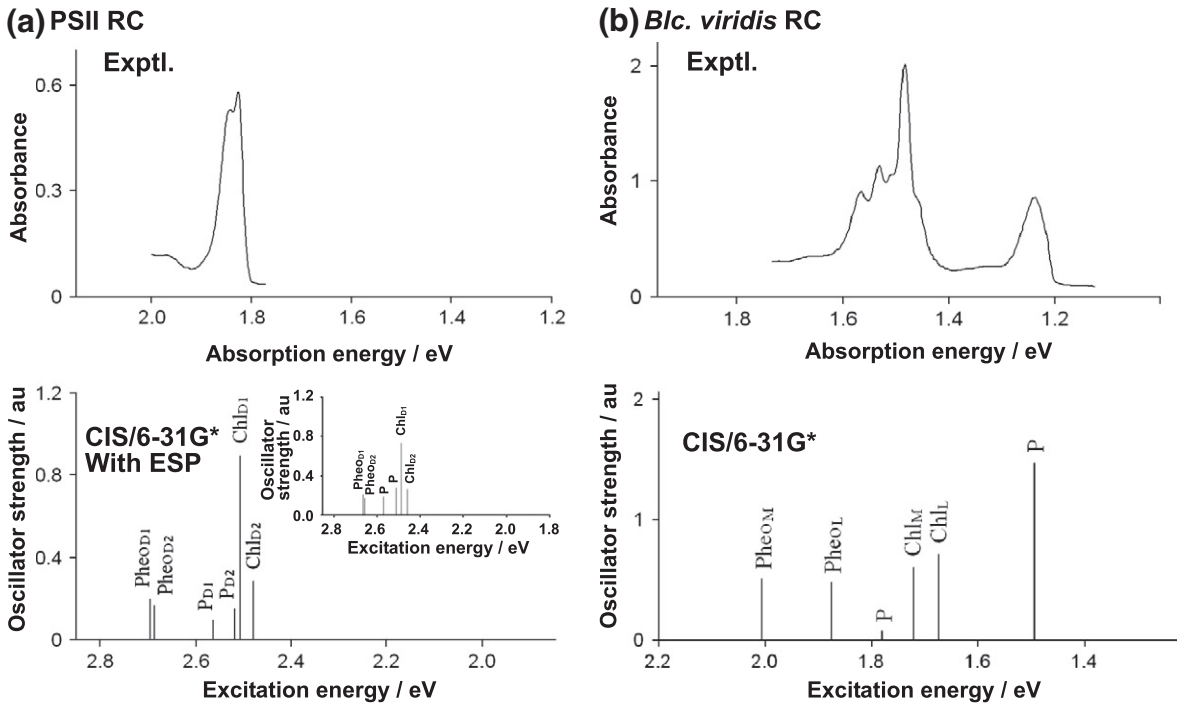

Fig. 2. (a) Experimental [12] and calculated absorption spectra of the PSII RC. The inset is a calculated spectrum without ESP. (b) Experimental [11] and calculated absorption spectra of the bRC. The calculated spectra of the PSII RC and the bRC were shifted by −0.65 eV and −0.25 eV, respectively, to match the first excitation energies in the experimental and calculated spectra.

using density-functional theory (DFT) at the B3LYP [29,30] /6-31G* level. As described in the Supplementary data, the root mean square deviations (RMSDs) were around 0.03 Å (Fig. S1). One exception is the geometry of the vinyl group in P_{D1} and P_{D2}: the distance between the vinyl group and the Mg^{2+} ion is so small. To correct these unphysical structures, the geometries of the vinyl groups were optimized using the B3LYP/6-31G* level. Later, we found the most recent X-ray structure [31] and confirmed that the optimized orientations of the vinyl group are reasonable. We also attached counter-ions to charged residues in the exterior of the protein to ensure that the total charge of the system is zero. The atomic coordinates, except for those of the chromophores, were optimized by molecular mechanics (MM) calculations with the TINKER [32] package. The AMBER99 force field [33] was used.

Chlorophylls and pheophytins have a phytyl group, as shown in Fig. 1 (b and c). In the present calculations for the excited states, the phytyl group was replaced by a methyl group. ESP from the rest of the phytyl group was considered with ESP-fitted charges (see more details in the Supplementary data). Chlorophylls are bound to the protein via a histidine residue. In the present model, the only electrostatic interaction with the imidazole ligand was included using atomic charges from the AMBER force field [33]. We also note that the phytyl group of P_{D1} comes close to the Chl_{D1} moiety. As a result of the simplification, this phytyl group was also described by ESP. To investigate how these simplifications affect the excitation energies, we included the phytyl group and the histidine ligand in the quantum chemical calculations. As shown in Table S1 in the Supplementary data, these simplifications caused minor changes in the excitation energy (within a deviation within 0.03 eV).

Regarding positions of the rest of hydrogen atoms of the chromophores in the RCs, we first performed MM calculations with the AMBER99 [33] force field and then semi-empirical PM3 [34] calculations to optimize the atomic coordinates.

The excited states of the chlorophyll hexamer in the RCs were calculated as a supermolecule to describe the molecular interactions at the ab initio level using Gaussian program [35]. We adopted the CI Singles (CIS) method with 6-31G* basis sets [36]. Because CIS is the simplest ab initio method for describing the excited states, only qualitative agreement is guaranteed. We did not discuss absolute excitation energy. In this paper, however, we are interested in the molecular interactions between the lowest singlet sates of chlorophyll monomers and in the energy splitting of the excited states caused by the interactions. To describe inter-molecular Coulomb interaction, character of the wave-function becomes critical. Because the main configurations and their coefficients of the CIS wave functions (Table 1) were in very good agreement with those of the symmetry-adapted cluster configuration interaction (SAC-CI) [37–40] wave functions [41], we expect that the calculated inter-molecular interactions and properties are reliable. In the SAC-CI wave function for the first excited state of Chlo *a* [41], the leading configuration was the HOMO to LUMO transition, and the coefficient was 0.81. In addition, B3LYP functional in DFT has a significant drawback in describing long-range Coulombic interactions [42]. Therefore, I think that CIS is the only method applicable to the present target. As shown in Fig. S3 of the Supplementary data, a time-dependent [43–45] density-functional theory [46] (TDDFT) calculation with the B3LYP functional [29,30] underestimates the excitation energies of the CT states among the chromophores, which is well known from previous studies [42,47,48]. In supplementary content, we included the Gaussian input files for the CIS calculations of the PSII RC with and without ESP.

3. Results and discussion

3.1. Absorption spectra of RCs

In Fig. 2, the calculated absorption spectra are compared with the experimental results [11,12]. Here, the system involved is only the RC, not the full PSII system. In Table 1, we also summarize the excited states of the RCs. Although the calculated excitation energies overshoot the experimental data, the results qualitatively reproduce the spectral shape of the experimental data. In particular, the present calculations clearly reproduce the prominent red-shift of the first excited state of the bRC, while no such shift appears in the PSII RC. Because our main goal is to understand why the spectral red-shift does not occur in the PSII, the present level of accuracy is satisfactory for this work. The systematic overestimation in the CIS result is due to

Table 1
Excited states of the PSII RC and the bRC.

State	PSII RC (*T. elongatus*)							bRC (*Blc.viridis*)		
	With protein effect				Without protein effect			Without protein effect		
	Character[a]	Main configurations[b]	E_{ex}[c]	f[d]	Character[a]	E_{ex}[c]	f[d]	Character[a]	E_{ex}[c]	f[d]
The first excited states of chlorophyll monomers in the SP										
	LE(P_{D1})	0.76(P_{D1}:H→L)	2.53	0.33	LE(P_{D1})	2.56	0.32	LE(P_L)	1.69	0.64
	LE(P_{D2})	0.76(P_{D2}:H→L)	2.53	0.31	LE(P_{D2})	2.52	0.31	LE(P_M)	1.71	0.65
Hexamer in RC										
2A	LE(Chl_{D2})	0.75(Chl_{D2}:H→L) +0.31(Chl_{D2}:H-1→L+1)	2.48	0.29	LE(Chl_{D2})	2.46	0.26	LE(P)	1.49	1.47
3A	LE(Chl_{D1})	0.59(Chl_{D1}:H→L) +0.42(P_{D2}:H→L)	2.51	0.89	LE(Chl_{D1})	2.49	0.73	LE(B_L)	1.67	0.71
4A	LE(P_{D2})	0.48(P_{D1}:H→L) −0.48(P_{D2}:H→L) +0.34(Chl_{D1}:H→L)	2.52	0.15	LE(P_{D2})	2.51	0.28	LE(B_M)	1.72	0.60
5A	LE(P_{D1})	0.55(P_{D1}:H→L) +0.35(P_{D2}:H→L)	2.56	0.10	LE(P_{D1})	2.57	0.18	LE(P)	1.78	0.07
6A	LE($Pheo_{D2}$)	0.66($Pheo_{D2}$:H→L) −0.45($Pheo_{D2}$:H-1→L)	2.68	0.17	LE($Pheo_{D1}$)	2.66	0.17	LE(H_L)	1.87	0.47
7A	LE($Pheo_{D1}$)	0.68($Pheo_{D1}$:H→L) −0.44($Pheo_{D1}$:H-1→L)	2.69	0.20	LE($Pheo_{D2}$)	2.67	0.21	LE(H_M)	2.01	0.51
14A	CT(Chl_{D1}→$Pheo_{D1}$)	0.98(Chl_{D1}:H→$Pheo_{D1}$:L)	3.68	0.00	CT(Chl_{D1}→$Pheo_{D1}$)	4.67	0.01	CT(B_L→H_L)	3.04	0.00
16A	CT(P_{D1}→$Pheo_{D1}$)	0.99(P_{D1}:H→$Pheo_{D1}$:L)	4.02	0.01						
19A	CT(P_{D2}→Chl_{D2})	0.89(P_{D2}:H→Chl_{D2}:L)	4.23	0.02						

[a] "LE" and "CT" denote locally excited state and charge transfer state, respectively.
[b] Configurations whose coefficients are larger than 0.3 (|C|>0.3) are shown. "H", "H-1", and "L" denotes HOMO, next HOMO, and LUMO, respectively.
[c] Excitation energy in eV.
[d] Oscillator strength in a.u.

the omission of electron correlation, which can be improved using correlated-excited-state methods.

In the case of bRC, the first excited state of the bacterial special pair (bSP), calculated at 1.49 eV, is a locally-excited state of the bacteriochlorophyll (BChl) dimer. The term "locally" means that the contribution from the inter-chromophore charge-transfer (CT) configuration is negligible. The representative configuration is an excitation from the highest occupied molecular orbital (HOMO, H) to the lowest unoccupied molecular orbital (LUMO, L) transition of the bSP. Here, the bSP is regarded as a single chromophore because the MOs are delocalized over the two BChls. In Table 1, we also show the first excitation energies of two BChls monomers, P_L and P_M, involved in bSP. The calculated excitation energies, 1.69 eV and 1.71 eV, clearly show that the lowest peak of bSP was red-shifted by 0.2 eV. The same conclusion was obtained in previous studies [49–51].

In contrast, four excited states (2^1A–5^1A states) of the PSII RC lie within 0.1 eV of each other, as shown in Fig. 2a. The calculated excitation energies are 2.48–2.56 eV, which are very similar to those of the chlorophyll monomers, 2.53 eV, as shown in Table 1. The 2^1A state, calculated at 2.46 eV, is dominated by the lowest excited state of Chl_{D2} (HOMO–LUMO transition). The CT components in the wave functions are negligible. In the 3^1A state, the locally-excited states of Chl_{D1} and P_{D2} are coupled in a wave function. We note that there is no such significant coupling between the excitations in the accessory chlorophyll and the bSP in bRC. Interestingly, the calculated oscillator strength is 0.89 a.u., which is more than twice as much as that of the monomers (0.31–0.33 a.u.). This increase in the oscillator strength is due to a J-type orientation of the TDM of the excited states. Here, by an analogy to the J-aggregate [52], we define the "J-type" orientation which reduces the absorption energy upon a dimer formation. We will describe some more details in a later subsection.

In the 4^1A and 5^1A states, we found that the HOMO–LUMO excited configurations of P_{D1} and P_{D2} are strongly coupled. However, the calculated excitation energies (2.52 and 2.56 eV) are very close to that of the Chl monomers (2.53 eV); this finding indicates that the interaction between P_{D1} and P_{D2} is small. Without the protein electrostatic effect, the calculated excitation energies of the 4^1A and 5^1A states become 2.51 eV and 2.57 eV, respectively, as shown in Table 1. These results indicate that the protein electrostatic effect does not control the spectral shift of the SP.

Comparing the 2^1A and 3^1A states, the energy of the chlorophyll in the D2 branch becomes lower than that of the D1 branch. This order is the same as that obtained by a previous study [16]. The important aspect pointed out was that the order of the states was relevant to the orientation of the vinyl group in ring I (see Fig. 1c) [16]. The orientation in Chl_{D1} is close to 90°, and the excitation energy of Chl_{D1} is 0.05 eV higher than that of Chl_{D2}. The π conjugation between the vinyl group and the chlorophyll macrocycle becomes stronger when the two units are in a more planar conformation. In the present case (the 2AXT structure [3]), the angle in Chl_{D1} and Chl_{D2} is 85° and 80°, respectively, and the calculated excitation energy was 2.49 eV and 2.46 eV, respectively.

Table 1 also shows some inter-chromophore CT states. The 14^1A, 16^1A, and 19^1A states are calculated at 3.68, 4.02, and 4.23 eV and characterized as CT from Chl_{D1} to $Pheo_{D1}$, P_{D1} to $Pheo_{D1}$, and P_{D2} to Chl_{D2}, respectively. The 14^1A state is involved in the electron transfer process in the RC, and the energy level is higher than that of the lowest singlet excited state (the 2^1A state) by 1.20 eV (27.7 kcal/mol). Here, the role of the protein ESP is very important. Without this protein effect, the excitation energy of the CT state is 4.67 eV, which is 2.21 eV (51.0 kcal/mol) above the 2^1A state. The ESP reduces the relative energy level by 23.3 kcal/mol. In contrast, the effect of the ESP on the excitation energies of the locally excited states is very small, 0.01–0.02 eV, as shown in Table 1. In another approach, we applied a self-consistent reaction field (SCRF) model with a polarized continuum model (PCM) [53]. A dielectric constant ε of cyclohexane (ε = 2.023) was used as in a previous study [50]. However, we could not obtain CT states below 4.17 eV as shown in Table S7 in the Supplementary data. The result indicates that the amount of the stabilization of the CT state was less than 0.5 eV. This result could be reasonable because the CT states (B_L→H_L) in bRC were stabilized by 0.4 eV when a SCRF model (ε = 2.0) was adopted in a previous study [50]. However, calculating the energy level of the CT state in condensed phase is still a difficult task in computational chemistry. Considering both the electrostatic and SCRF effects, the CT states may appear in a reasonably lower-energy region.

As shown in Fig. 3(a and b), the cause of the stabilization of the 14^1A state (Chl_{D1}→$Pheo_{D1}$) is that the ESP around $Pheo_{D1}$ is more

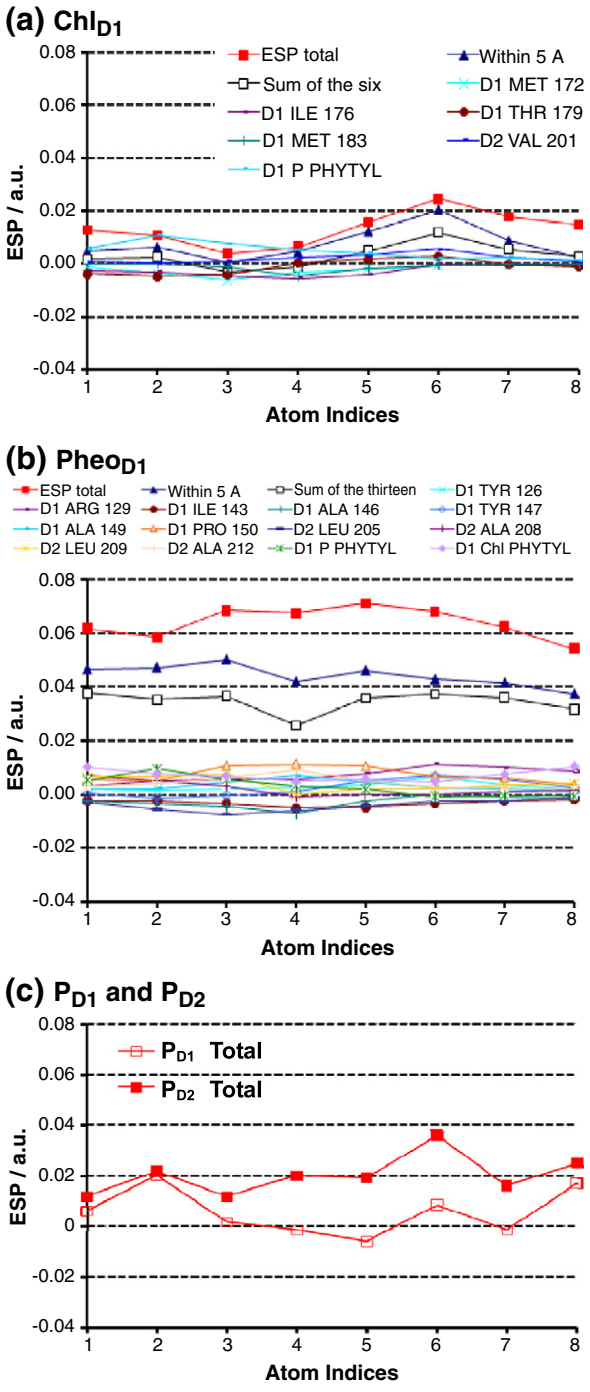

Fig. 3. ESP of the RC protein calculated at the conjugated atoms in the chlorophyll rings (red lines) of (a) Chl$_{D1}$, (b) Pheo$_{D1}$, and (c) P$_{D1}$ and P$_{D2}$. See Fig. 2 for the atom indices. Amino acids whose contributions are larger than 0.005 a.u. in absolute value are also shown. Open squares (□) in black are the sum of the amino-acid contributions shown in each figure. Filled triangles (▲) in dark blue are the sum of the contributions from amino acids within 5 Å of the chromophore.

positive than that around Chl$_{D1}$. The red lines in Fig. 3 are the total ESP from the protein. The calculated ESP around Pheo$_{D1}$ is 0.05–0.07 a.u., while that around Chl$_{D1}$ is 0.01–0.03 a.u. To understand the origin of this difference, the calculated ESP was decomposed into amino acid contributions. As shown in Fig. 3, there is no specific amino acid that characterizes the total ESP lines for both Chl$_{D1}$ and Pheo$_{D1}$. By summing these contributions, the ESP line approaches the total. The dark blue lines in Fig. 3(a and b) show contributions from amino acids within 5 Å of the chromophore. The dark line behaves similarly to the red line, indicating that small ESP contributions close to the chromophore produce the difference in the total ESP. In the Pheo$_{D1}$ case, however, roughly 30% of total ESP arises from amino acids more than 5 Å away from the chromophore. This effect is due to the other charged amino acids in the hydrophilic region of the RC on the stroma side.

3.2. Molecular interactions and spectral intensity

In this subsection, we show that the wave functions of the excited states are described by a linear combination of the monomer excitons. In Table 2, the CI coefficients of the excited-state wave function are compared with those of the monomers. The ratio of the CI coefficients in the monomer wave function is very well conserved in the 6-mer wave function. The relative values of the CI coefficients are also summarized in Table S2 in the Supplementary data. In the case of the 2^1A state of the 6-mer, the relative CI coefficients for the H→L, H→L+1, H-1→L, and H-1→L+1 excitations of the P$_{D1}$ moiety are 1.00, 0.41, −0.35, and 0.24, respectively. These values are very similar to those in the P$_{D1}$ monomer, which are 1.00, 0.49, −0.49, and 0.37 for the H→L, H→L+1, H-1→L, and H-1→L+1 excitations, respectively. We note that the excited configurations of the 6-mer can be easily assigned to an excited configuration of the monomer wave functions because the molecular orbitals of the 6-mer are localized on each monomer, as shown in Table S4 of the Supplementary data. These results provide theoretical computational support for the applicability of the exciton theoretical approach adopted in previous theoretical works [13–18].

Next, we show how the molecular interactions relate to the spectral intensity. With the original CIS coefficients shown in Table 2, the wave functions can be simplified as follows (see the Supplementary data).

$$\Psi^{2^1A} = 0.22\Phi^{P_{D1}} + 0.24\Phi^{P_{D2}} + 0.14\Phi^{Chl_{D1}} + 0.93\Phi^{Chl_{D2}} \quad (1)$$

$$\Psi^{3^1A} = -0.04\Phi^{P_{D1}} + 0.55\Phi^{P_{D2}} + 0.76\Phi^{Chl_{D1}} - 0.25\Phi^{Chl_{D2}} \quad (2)$$

$$\Psi^{4^1A} = 0.63\Phi^{P_{D1}} - 0.63\Phi^{P_{D2}} + 0.44\Phi^{Chl_{D1}} - 0.04\Phi^{Chl_{D2}} \quad (3)$$

$$\Psi^{5^1A} = 0.72\Phi^{P_{D1}} + 0.46\Phi^{P_{D2}} - 0.35\Phi^{Chl_{D1}} - 0.21\Phi^{Chl_{D2}} \quad (4)$$

The configurations $\Phi^{P_{D1}}$, $\Phi^{P_{D2}}$, $\Phi^{Chl_{D1}}$, and $\Phi^{Chl_{D2}}$ are the contracted wave functions of the locally excited states of monomers.

With these simplified wave functions, the electric transition dipole moment (TDM) of the excitations was recomputed as $\sum_I^M C^I \langle \Phi^J | \hat{r} | \Phi^g \rangle$ using the monomer TDM, $\langle \Phi^J | \hat{r} | \Phi^g \rangle$, where the index I stands for P$_{D1}$, P$_{D2}$, Chl$_{D1}$, Chl$_{D2}$, Pheo$_{D1}$, and Pheo$_{D2}$. $|\Phi^g\rangle$ stands for the ground-state wave function. C^I is the coefficient shown in Eqs. (1)–(4). The results are summarized in Fig. 4. The TDM calculated with the contracted wave function (black) reproduced that of the original 6-mer wave function (gray). This result also indicates that the wave function of the 6-mer is a linear combination of the first excited state of the monomers. It is very clear that in the 3^1A state, the TDMs of the first excited states of Chl$_{D1}$, P$_{D2}$, and Chl$_{D2}$ together increase the total TDM of the state. The wave function of the 4^1A state corresponds to the lowest excited state of the SP in the PSII RC. Although the TDMs of P$_{D1}$ and P$_{D2}$ give additive contributions, the TDM of Chl$_{D1}$ destructively interferes with those of P$_{D1}$ and P$_{D2}$. The resultant TDM of the state is similar to that of the monomer. The 5^1A state also shows destructive interference among the monomer transitions.

In the following, the origin of the constructive/destructive interference of TDM is discussed. We adopt a two-state model that considers the interaction between the excited states of two monomers (see the Supplementary data for more details). The wave function of the two-state model Ψ is expressed by a linear combination of the first excited states of the monomers, such as $\Psi = c_1\Phi_1 + c_2\Phi_2$. With the analytical solution of the two-dimensional Schrödinger equation, the ratio of the

Table 2
Wave functions of the excited states of the PSII RC.

Chr.[a]	Config.[b]	Coefficients							
		First excited state of monomer[c]				Excited states of 6-mer			
		P_{D1}	P_{D2}	Chl_{D1}	Chl_{D2}	2^1A	3^1A	4^1A	5^1A
P_{D1}	H→L	0.76				0.17	−0.03	0.48	0.55
	H→L+1	0.37				0.07	−0.03	0.21	0.28
	H-1→L	−0.37				−0.06	0.03	−0.24	−0.28
	H-1→L+1	0.28				0.04		0.17	0.21
P_{D2}	H→L		0.76			0.18	0.42	−0.48	0.35
	H→L+1		0.35			0.08	0.18	−0.21	0.18
	H-1→L		−0.37			−0.07	−0.20	0.24	−0.20
	H-1→L+1		0.30			0.07	0.14	−0.17	0.16
Chl_{D1}	H→L			0.78		0.11	0.59	0.34	−0.27
	H→L+1			0.34		0.06	0.25	0.16	−0.11
	H-1→L			−0.34		−0.04	−0.24	−0.13	0.13
	H-1→L+1			0.33		0.04	0.24	0.14	−0.13
Chl_{D2}	H→L				0.81	0.75	−0.20	−0.03	−0.17
	H→L+1				0.30	0.30	−0.07	−0.03	−0.07
	H-1→L				−0.30	−0.28	0.08		0.08
	H-1→L+1				0.35	0.31	−0.08		−0.08

[a] Chromophores.
[b] Configurations. "H,", "H-1", "L", and "L+1" denote HOMO, next-HOMO, LUMO, and next-LUMO, respectively.
[c] Calculations performed with protein ESP.

coefficients, c_1/c_2, is expressed by two parameters, ΔE and V. In Fig. 5, the ratio of the first excited state is mapped on a ΔE vs. V plane (called the $\Delta E - V$ plane hereafter). ΔE, defined as $E_1 - E_2$, is the difference in the excitation energies of the two states Φ_1 and Φ_2. The dark region ($0.5 \leq |c_1/c_2| \leq 2.0$) indicates the degeneracy of the two components and distributes around the $\Delta E = 0$ axis. V is the Coulombic interaction between the two states. The sign of V determines the ratio c_1/c_2 and, therefore, controls whether the interference of the two TDMs is constructive or destructive.

If $V<0$, where the ratio c_1/c_2 becomes positive, an acute angle between two TDMs ($0° < \theta < 90°$) leads to constructive interference in the first excited state. In the second excited state, the interference becomes destructive because the sign of the ratio becomes inverted as a consequence of the configuration interaction. As shown in Fig. 5, the Chl_{D1}–P_{D2} pair falls into this classification because the pair is in the degenerate region with an acute θ angle (9.8°). The orientation of the Chl_{D1}–P_{D2} pair could also be characterized as a J-type orientation. A pair of TDM in the J-type orientation causes a red-shifted absorption peak compared with that of the monomer [52]. In contrast, we define an H-type orientation of TDMs when a blue-shift occurs in the absorption peak. A positive V value leads to a negative ratio, $c_1/c_2<0$, and, therefore, an obtuse angle ($90° < \theta < 180°$) causes a constructive interference. This could also be considered as a J-type orientation. The P_{D1}–P_{D2} and Chl_{D1}–Chl_{D2} pairs are classified into this category, as shown in Fig. 5.

The results of the analysis clearly explain the magnitude of the TDMs of the excited states. The 3^1A state has the largest moment because the Chl_{D1}–P_{D2} pair in the J-type orientation gives large contributions to the total TDM. Although the TDM of Chl_{D2} also contributes, as seen in Fig. 4b, the contribution is small because both of the Chl_{D1}–Chl_{D2} and P_{D2}–Chl_{D2} pairs are not in the degenerate region due to the difference in excitation

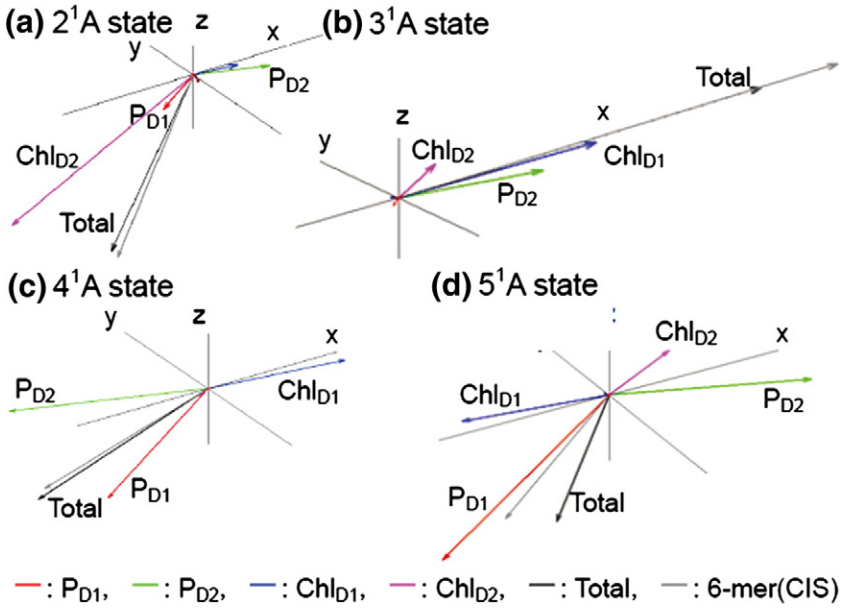

Fig. 4. Direction of the transition dipole moment (TDM) of (a) 2^1A, (b) 3^1A, (c) 4^1A, and (d) 5^1A states and their monomer components. The term "total" indicates the sum of the TDMs of the six monomers, and "6-mer (CIS)" denotes the TDMs calculated with the CIS wave function of the 6-mer.

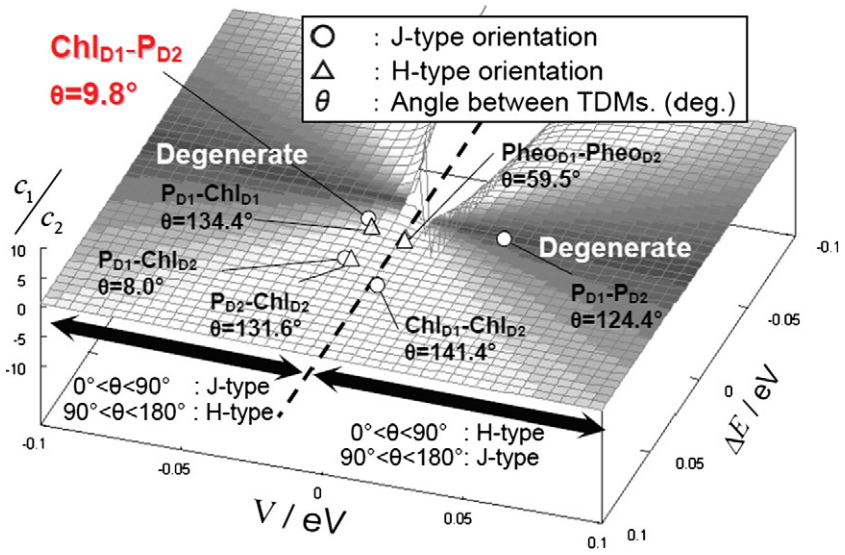

Fig. 5. The C_1/C_2 plot for the first excited state of the chromophore pairs in the PSII RC. As the degeneracy increases, the surface becomes darker. The angles between the transition dipole moments (θ) determine the type of the orientation of the two chromophores. In the first excited state, if $V>0$, acute ($0°<\theta<90°$) and obtuse ($90°<\theta<180°$) angles indicate H- and J-type orientations, respectively. In contrast, when $s<0$, acute ($0°<\theta<90°$) and obtuse ($90°<\theta<180°$) angles indicate J- and H-type orientations, respectively.

energy (ΔE). Although the P_{D1}–Chl_{D2} pair is a counter-pair to the Chl_{D1}–P_{D2} pair, their constructive interference seen in the 2^1A state is small. The cause of this phenomenon lies in the difference excitation energy (ΔE), as seen in Fig. 5. In the case of the bRC, the TDM of the first excited state of the bSP is the largest [51]. In the case of the PSII RC, however, the TDM of the excited state of the SP (4^1A state) is similar to that of the monomer. Although the P_{D1}–P_{D2} pair is in the degenerate region and in a J-type orientation, the P_{D2}–Chl_{D1} pair has a destructive contribution because the 4^1A state is also characterized as a combination of the first excited state of P_{D1} and the second excited state of the Chl_{D1}–P_{D2} pair. Because the Chl_{D1}–P_{D2} pair is in a J-type orientation, there is only a small TDM in the second excited state.

3.3. Chromophore orientation and excitation energies

As described in the previous subsection, the calculated excitation energies are rather insensitive to the protein ESP, as shown in Table 1. To understand the origin of the red-shift from a structural standpoint, we next compare the chromophore orientation of the PSII RC with that of the bRC.

Fig. 6 shows the structural similarities and deviation between the SPs. The atomic coordinates of the PSII RC were rotated and shifted to minimize the deviations between P_L in the bRC and P_{D1} in the PSII RC. For the bRC (shown in red), two chlorophylls are symmetrically aligned in a pseudo-C_2 point group. In the PSII RC, the position of P_{D2} rotates in a clockwise manner, as seen in Fig. 6(a), which was identified in a previous study [18]. The distance between the Cβ′ atoms (Ring II) of P_L and P_{D2} is 1.95 Å and is the largest among the atoms in the chlorophyll ring. On the other hand, the deviation in the interplanar distance is not very significant, as seen in Fig. 6(b). The averaged interplanar distances are 3.70 Å and 3.48 Å in the PSII RC and the bRC, respectively. Fig. 6(b) also shows that the positions of the accessory chlorophylls in PSII RC are 1.0 Å closer to the SP. This difference could be the cause of the strong coupling between the excitations of Chl_{D1} and P_{D2}, as seen in Table 1. Regarding the positions of pheophytins relative to accessory chlorophylls, the calculated deviation is very small, as shown in Fig. S7(c and d).

These observations indicate that the major difference in the chromophore orientation occurs in P_{D1}, P_{D2}, Chl_{D1}, and Chl_{D2}. Therefore, we performed CIS/6-31G* calculations for the four chlorophylls (4-mer) to investigate how the chromophore orientation affects their excitation energies (for a schematic illustration, see Fig. S8 in the Supplementary data). First, the atomic coordinates of the 6-mer model, which were based on the X-ray structure [3], were used for these four chlorophylls (Model 0 in Fig. S8(a)). In Model 1 (Fig. S8(b)), the positions of the two accessory chlorophylls are moved to the bRC-like position. Least-square deviations

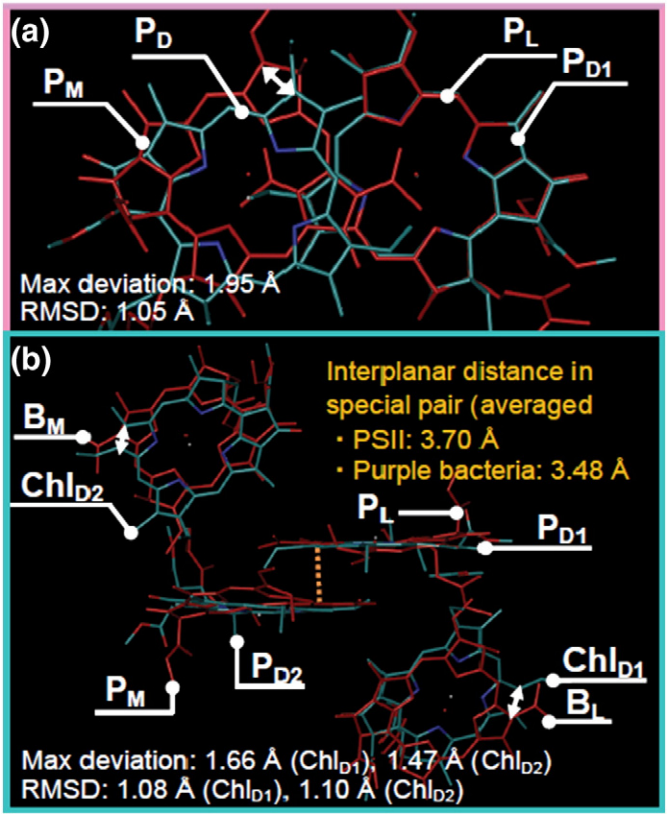

Fig. 6. Chromophore orientation in the PSII RC (colored by element) and the bRC (red). In (a) and (b), P_{D1} and P_L are superimposed to minimize the positional deviation of the four N atoms, C2, C8, and four C atoms in Ring I (see Fig. 1 for atom indices). RMSD and max deviation were measured for the atoms in the chlorophyll ring. White arrows indicate the max deviation. In (b), an averaged interplanar distance in the SP was also calculated. For the PSII RC, Cα(ring II of P_{D2}) – C2(P_{D1}), C2(P_{D2}) – Cα′(ring I of P_{D1}), and Cβ′(ring I of P_{D2}) – Cα(ring I of P_{D1}) pairs overlap relatively well and their distances were measured. For the bRC, the distances of the six atom pairs (the C and N atoms of the Ring I and the C2 atom) was averaged to define the interplanar distance between P_L and P_M. ProFit [58] and VMD [59] were used for the fitting procedures and for the graphics, respectively.

for the four N atoms were minimized. In Model 2 (Fig. S8(c)), P_{D2} was moved to the P_M-like position in the bRC. In Model 3 (Fig. S8(d)), P_{D2}, Chl_{D1}, and Chl_{D2} were moved to the positions of the corresponding chromophores in the bRC.

The calculated excitation energy with the PSII orientation (2.52 eV) red-shifts to 2.39 eV when the bRC-like orientation (Models 2 and 3) is adopted. The excitation energy of the 4-mer significantly decreases by 0.13 eV when P_{D2} orientation in the SP is changed to the bRC-like position. The shift is comparable to that in the bRC (0.20 eV). In contrast, little change occurs when the relative positions of the accessory chlorophylls are modified. It is very clear that the orientation of P_{D1} and P_{D2} causes spectral shift in the SP of PSII RC.

We also found that orientation of the accessory chlorophylls is important for the configuration mixing between Chl_{D1} and P_{D2} in the 3^1A state. In the 6-mer model and in Model 0, the excited configurations of P_{D2} are around 30% and 23%, respectively. The weight decreases to 8% when Chl_{D1} and Chl_{D2} are moved to the bRC-like orientation. Therefore, the large transition moment in the 3^1A state originates from the orientation of the accessory chlorophylls.

To figure out why the orientation affects the excitation energy, we investigated how the MOs and their energy levels change after the orientation is modified. Calculations were performed without including the protein environment. As clearly shown by the orange lines in Fig. 7, the HOMO level increased by 0.077 eV and the LUMO level decreased by 0.194 eV after the modification. The calculated HOMO–LUMO gap in the PSII orientation (6.03 eV) decreased to 5.76 eV. This result clearly shows that the monomer orientation of the bRC type provides a greater orbital interaction than that of the PSII type. Fig. 7 also shows the HOMO and LUMO levels of P_{D1} and P_{D2} calculated as monomer. The HOMO–LUMO gap is 6.09 eV and 6.04 eV for P_{D1} and P_{D2}, respectively. Interestingly, the SP formation in the PSII RC has a very minor effect on the orbital energies. This effect is ascribed to asymmetric dimer formation. As shown in Fig. 7, bonding and anti-bonding interactions co-exist in the orbital interaction for the PSII system. On the other hand, symmetric dimer formation in the bRC causes the bonding interaction in the next-HOMO and the LUMO, while the anti-bonding interaction appears in the HOMO and the next-LUMO. We also note that the MOs tend to delocalize without the protein electrostatic effect. Therefore, both the protein ESP and asymmetric dimer formation contribute to the similarity between the orbital levels of the SP and those of the monomers.

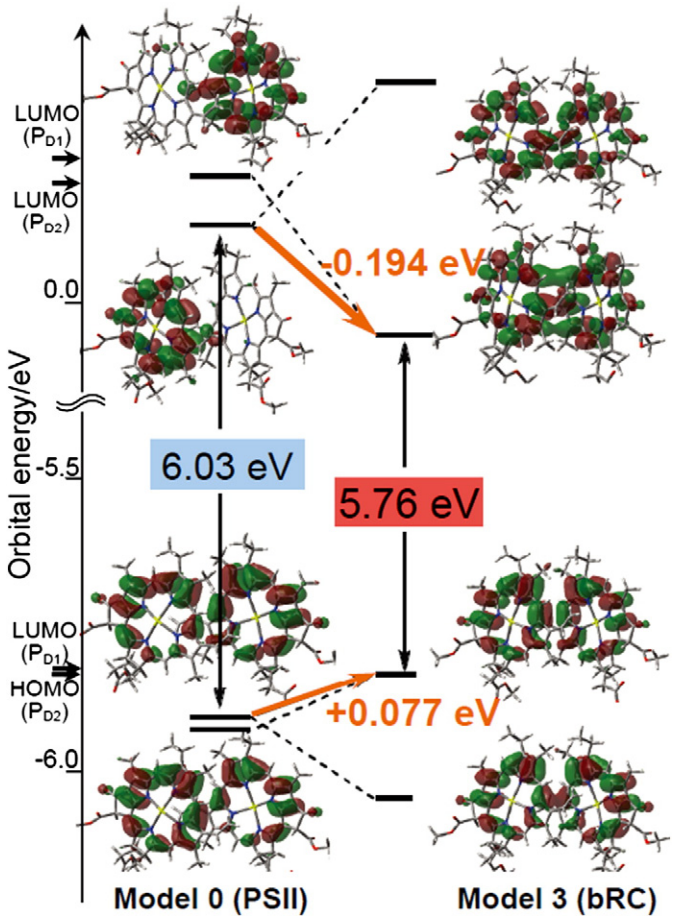

Fig. 7. Orbital energies of the SP in the PSII-type and bRC-type orientations.

3.4. Protein structural origin of the P_{D2} displacement in PSII

Compared with the symmetric dimer formation in the bRC case, the displacement of P_{D2} to the asymmetric position diminishes the orbital interaction between P_{D1} and P_{D2}. To understand the protein structural origin of the P_{D2} displacement, we compared several helices close to P_{D2} with those of the bRC. We transformed the atomic coordinates of the PSII RC to minimize the structural deviations between P_L in the bRC and P_{D1} in the PSII RC (see the Supplementary data).

As shown in Fig. 8 and Fig. S5(a), the displacement of P_{D2} is best correlated to that of the CD helix. The large displacement vectors in P_{D2} have similar directions to those of the CD helix. On the other hand, the displacements of the C, D, and E helices are less correlated to those of P_{D2} (see Fig. S5 in Supplementary data). Although P_{D2} is bound to the D helix via His197, only the side-chain of His197 is correlated to the displacement of P_{D2}, as shown in Fig. S5(c). From a viewpoint of molecular evolution, the spectral change of the PSII RC could originate from natural mutations that shifted the CD helix.

3.5. Asymmetric protein electrostatic effect on the ionization potential of the SP

Before closing the present report, we will mention the protein ESP effect on the ionization potential (IP). The PSII RC has an IP that is higher than that of the bRC to oxidize water molecule. As we described in the previous section, the protein ESP very slightly changes the absorption spectrum except for the energy levels of the charge-transfer states.

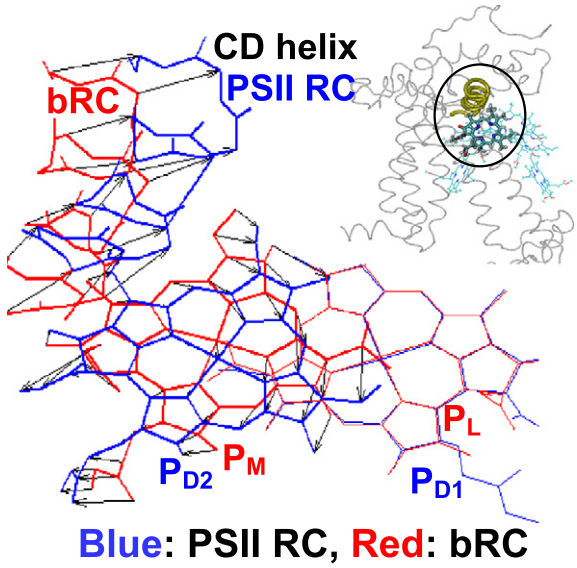

Fig. 8. Correlation between the displacements of P_{D2} and the CD helix. Insets show the position of P_{D2} and the CD helix (yellow) in the D2 subunit of the RC protein.

However, there are two points that are interesting to note. First, the ESP localizes the HOMO distributions of P_{D1} and P_{D2}. In the gas phase results shown in Fig. 7 and in a previous report with a continuum model [26], the HOMO is delocalized over P_{D1} and P_{D2}, the SP. With the protein ESP, the HOMO of PSII RC distributes locally on P_{D1}, as shown in Fig. S4 in the Supplementary data. This result agrees with previous experimental results [54–56]. Second, the ESP changes the HOMO level from −6.01 eV to −6.33 eV. The amount of stabilization (0.3 eV) is close to that reported in a previous theoretical study [57]. These two points have the same origin. Because the ESP value in the P_{D2} moiety is larger than that in the P_{D1} moiety (Fig. 3(c)), the orbital energy levels of P_{D2} are stabilized more than those of P_{D1}. This breakdown of the degeneracy causes orbital localization within the monomer moiety. At the same time, positive ESP increases the IPs of P_{D1} and P_{D2}.

4. Conclusions

We performed ab initio quantum chemical calculations for the excited states of the chlorophyll 6-mer at the CIS/6-31G* level to investigate the electronic structures of the excited states of the PSII RC and the bRC and to clarify the origin of the differences. We also investigated the effect of the protein electrostatic potential (ESP) on the excited states and the ionization potential of the PSII RC.

First, asymmetric orientation in the SP formation is the origin of the difference in the lowest peak of the absorption spectra. Although SP in the bRC has a pseudo-C_2 axis, P_{D2} in PSII RC is rotated clockwise, as shown in Fig. 6(a). Because of this asymmetry, both bonding and anti-bonding interactions co-exist and weaken the orbital interaction between P_{D1} and P_{D2}. This orientation can be traced back to the structural difference in the CD helix between the two RCs.

Second, the electronic structure of the low-lying excited states of the PSII RC is characterized as a linear combination of the exciton states of the chlorophyll monomers. This conclusion verifies the applicability of the exciton theory to the PSII problems. The transition dipole moment (TDM) of the transitions, which is related to the intensity of the absorption spectrum, is also described well with the linear combination of the monomer TDM vectors. To understand the interferences among the monomer TDMs, we introduced a diagram that maps the wave function degeneracy on the ΔE-V plane. Together with the angle between the TDMs, this diagram can rationalize constructive/destructive interference and explain the magnitude of the TDM of the excited states.

Finally, the effect of the protein ESP on the charge-transfer (CT) states and ionization potential (IP) are clarified. The ESP stabilizes the energy of CT from Chl_{D1} to $Pheo_{D1}$ by roughly 1.0 eV. Because the magnitude of the ESP is not uniform around the SP, the HOMO distribution is localized to the P_{D1} moiety, which explains the results of previous experiments [54–56]. Because the ESP is positive, the HOMO level becomes deeper, and the IP increases by 0.3 eV, which is similar to the result of a previous electrostatic calculation [57].

Acknowledgments

This study was supported by KAKENHI (no. 21685002) from the Japan Society for the Promotion of Science (JSPS). This study was also supported by the JST-CREST and by a Grant-in-Aid for Young Scientists from the ACCMS and IIMC, Kyoto University. A portion of the computations was conducted at the RCCS (Okazaki, Japan).

Appendix A. Supplementary data

Supplementary data to this article can be found online at 10.1016/j.bpc.2011.06.011.

References

[1] B.A. Diner, F. Rappaport, Structure, dynamics, and energetics of the primary photochemistry of photosystem II of oxygenic photosynthesis, Annu. Rev. Plant Biol. 53 (2002) 551–580.
[2] G. Renger, A.R. Hozwarth, Primary electron transfer, in: T. Wydrzynski, K. Satoh (Eds.), Photosystem II: The Light-Driven Water Plastquinone Oxidoreductase, Springer, Dordrecht, The Netherlands, 2005.
[3] B. Loll, J. Kern, W. Saenger, A. Zouni, J. Biesiadka, Towards complete cofactor arrangement in the 3.0 Å resolution structure of photosystem II, Nature 438 (2005) 1040–1044.
[4] O. Nanba, K. Satoh, Isolation of a photosystem II reaction center consisting of D-1 and D-2 polypeptides and cytochrome b-559, Proc. Natl. Acad. Sci. U. S. A. 84 (1987) 109–112.
[5] H. Michel, J. Deisenhofer, Relevance of the photosynthetic reaction center from purple bacteria to the structure of photosystem II, Biochemistry 27 (1988) 1–7.
[6] A.W. Rutherford, P. Faller, Photosystem II: evolutionary perspectives, Philos. Trans. R. Soc. London, B 358 (2002) 245–253.
[7] A.W. Rutherford, W. Nitschke, Photosystem II and the quinone-iron-containing reaction centers: comparisons and evolutionary perspectives, in: H. Baltsheffsky (Ed.), Origin and Evolution of Biological Energy Conversion, VCH, New York, 1996, pp. 143–175.
[8] A.Y. Shkuropatov, R.A. Khatypov, T.S. Volshchukova, V.A. Shkuropatova, T.G. Owens, V.A. Shuvalov, Spectral and photochemical properties of borohydride-treated D1-D2-cytochrome b-559 complex of photosystem II, FEBS Lett. 420 (1997) 171–174.
[9] A.Y. Shkuropatov, R.A. Khatypov, V.A. Shkuropatova, M.G. Zvereva, T.G. Owens, V.A. Shuvalov, Reaction centers of photosystem II with a chemically-modified pigment composition: exchange of pheophytins with 13^1-deoxo-13^1-hydroxy-pheophytin *a*, FEBS Lett. 450 (1999) 163–167.
[10] J. Breton, Orientation of chromophores in the reaction center of *Rhodopseudomonas viridis*. Comparison of low-temperature linear dichroism spectra with a model derived from X-ray crystallography, Biochim. Biophys. Acta 810 (1985) 235–245.
[11] D. Tang, R. Jankowiak, G.J. Small, Structured hole burned spectra of the primary donor state absorption region of *Rhodopseudomonas viridis*, Chem. Phys. 131 (1989) 99–113.
[12] V.I. Prokhorenko, A.R. Holzwarth, Primary processes and structure of the photosystem II reaction center: a photon echo study, J. Phys. Chem. B 104 (2000) 11563–11578.
[13] S. Vasil'ev, P. Orth, A. Zouni, T.G. Owens, D. Bruce, Excited-state dynamics in photosystem II: insights from the X-ray crystal structure, Proc. Natl. Acad. Sci. U. S. A. 98 (2001) 8602–8607.
[14] J.R. Durrant, D.R. Klug, S.L.S. Kwa, R.v. Grondelle, A multimer model for P680, the primary electron donor of photosystem II, Proc. Nat. Acad. Sci. U. S. A. 92 (1995) 4798–4802.
[15] L.M.C. Barter, J.R. Durrant, D.R. Klug, A quantitative structure–function relationship for the PSII reaction center: supermolecular behavior in natural photosynthesis, Proc. Natl. Acad. Sci. U. S. A. 100 (2003) 946–951.
[16] N. Ivashin, S. Larsson, Excitonic states in photosystem II reaction center, J. Phys. Chem. B 109 (2005) 23051–23060.
[17] G. Raszewski, W. Saenger, T. Renger, Theory of optical spectra of photosystem II reaction centers: location of the triplet state and the identity of the primary electron donor, Biophys. J. 88 (2005) 986–998.
[18] G. Raszewski, B.A. Diner, E. Schlodder, T. Renger, Spectroscopic properties of reaction center pigments in photosystem II core complexes: revision of the multimer model, Biophys. J. 95 (2008) 105–119.
[19] A. Zouni, H.-T. Witt, J. Kern, P. Fromme, N. Krau, W. Saenger, P. Orth, Crystal structure of photosystem II from *Synechococcus elongatus* at 3.8 Å resolution, Nature 409 (2001) 739–743.
[20] S.A.P. Merry, S. Kumazaki, Y. Tachibana, D.M. Joseph, G. Porter, K. Yoshihara, J. Barber, J.R. Durrant, D.R. Klug, Sub-picosecond equilibration of excitation energy in isolated photosystem II reaction centers revisited: time-dependent anisotropy, J. Phys. Chem. 100 (1996) 10469–10478.
[21] S. Vasil'ev, D. Bruce, A protein dynamics study of Photosystem II; the effects of protein conformation on reaction center function, Biophys. J. 90 (2006) 3062–3073.
[22] S. Yin, M.G. Dahlbom, P.J. Canfield, N.S. Hush, R. Kobayashi, J.R. Reimers, Assignment of the Qy absorption spectrum of photosystem-I from *Thermosynechoccus elongatus* based on CAM-B3LYP calculations at the PW91-optimized protein structure, J. Phys. Chem. B 111 (2007) 9923–9930.
[23] M.E. Madjet, H. Müh, T. Renger, Deciphering the influence of short-range electronic coupling on optical properties of molecular dimers: application to "special pairs" in photosynthesis, J. Phys. Chem. B 113 (2009) 12603–12614.
[24] M.E. Madjet, A. Abdurahman, T. Renger, Intermolecular Coulomb coupling from *ab initio* electrostatic potentials: application to optical transitions of strongly coupled pigments in photosynthetic antennae and reaction centers, J. Phys. Chem. B 110 (2006) 17268–17281.
[25] S. Larsson, Electron transfer in chemical and biological systems. Orbital rules for nonadiabatic transfer, J. Am. Chem. Soc. 103 (1981) 4034–4040.
[26] R. Takahashi, K. Hasegawa, T. Noguchi, Effect of charge distribution over a chlorophyll dimer on the redox potential of P680 in Photosystem II as studied by density functional theory calculations, Biochemistry 47 (2008) 6289–6291.
[27] C.R.D. Lancaster, H. Michel, The coupling of light-induced electron transfer and proton uptake as derived from crystal structures of reaction centres from *Rhodopseudomonas viridis* modified at the binding site of the secondary quinone, QB, Structure 5 (1997) 1339–1359.

[28] P. Canfield, M.G. Dahlbom, N.S. Hush, J.R. Reimers, Density-functional geometry optimization of the 150000-atom photosystem-I trimer, J. Chem. Phys. 124 (2006) 024301.
[29] C. Lee, W. Yang, R.G. Parr, Development of the Colle–Salvetti correlation-energy formula into a functional of the electron density, Phys. Rev. B 37 (1988) 785.
[30] A.D. Becke, Density-functional thermochemistry. III. The role of exact exchange, J. Chem. Phys. 98 (1993) 5648–5652.
[31] A. Guskov, J. Kern, A. Gabdulkhakov, M. Broser, A. Zouni, W. Saenger, Cyanobacterial photosystem II at 2.9 Å resolution and the role of quinones, lipids, channels and chloride, Nat. Struct. Mol. Biol. 16 (2009) 334–342.
[32] J.W. Ponder, F.M. Richards, An efficient Newton-like method for molecular mechanics energy minimization of large molecules, J. Comput. Chem. 8 (1987) 1016–1026.
[33] J. Wang, P. Cieplak, P.A. Kollman, How well does a restrained electrostatic potential (resp) model perform in calculating conformational energies of organic and biological molecules, J. Comput. Chem. 21 (2000) 1049–1074.
[34] J.J.P. Stewart, Optimization of parameters for semiempirical methods I. Method, J. Comput. Chem. 10 (1989) 209–220.
[35] M.J. Frisch, G.W. Trucks, H.B. Schlegel, G.E. Scuseria, M.A. Robb, J.R.J.A. Cheeseman, J. Montgomery, T. Vreven, K.N. Kudin, J.C. Burant, J.M. Millam, S.S. Iyengar, J. Tomasi, V. Barone, B. Mennucci, M. Cossi, G. Scalmani, N. Rega, G.A. Petersson, H. Nakatsuji, M. Hada, M. Ehara, K. Toyota, R. Fukuda, J. Hasegawa, M. Ishida, T. Nakajima, Y. Honda, O. Kitao, H. Nakai, M. Klene, X. Li, J.E. Knox, H.P. Hratchian, J.B. Cross, C. Adamo, J. Jaramillo, R. Gomperts, R.E. Stratmann, O. Yazyev, A.J. Austin, R. Cammi, C. Pomelli, J. Ochterski, P.Y. Ayala, K. Morokuma, G. Voth, P. Salvador, J.J. Dannenberg, V.G. Zakrzewski, S. Dapprich, A.D. Daniels, M.C. Strain, O. Farkas, D.K. Malick, A.D. Rabuck, K. Raghavachari, J.B. Foresman, J.V. Ortiz, Q. Cui, A.G. Baboul, S. Clifford, J. Cioslowski, B.B. Stefanov, G. Liu, A. Liashenko, P. Piskorz, I. Komaromi, R.L. Martin, D.J. Fox, T. Keith, M.A. Al-Laham, C.Y. Peng, A. Nanayakkara, M. Challacombe, P.M.W. Gill, B. Johnson, W. Chen, M.W. Wong, C. Gonzalez, J.A. Pople, Gaussian03, Gaussian, Inc., Pittsburgh, PA, 2003.
[36] W.J. Hehre, R. Ditchfield, J.A. Pople, Self-consistent molecular orbital methods. XII. Further extensions of Gaussian-type basis sets for use in molecular orbital studies of organic molecules, J. Chem. Phys. 56 (1972) 2257–2261.
[37] H. Nakatsuji, Cluster expansion of the wavefunction. Excited States, Chem. Phys. Lett. 59 (1978) 362.
[38] H. Nakatsuji, Cluster expansion of the wavefunction. Calculation of electron correlations in Ground and excited states by SAC and SAC-CI theories, Chem. Phys. Lett. 67 (1979) 334.
[39] H. Nakatsuji, Cluster expansion of the wavefunction. Electron correlations in ground and excited states by SAC (symmetry-adapted-cluster) and SAC-CI theories, Chem. Phys. Lett. 67 (1979) 329.
[40] H. Nakatsuji, SAC-CI method: theoretical aspects and some recent topics, in: J. Leszczynski (Ed.), Computational Chemistry — Reviews of Current Trends, 2, World Scientific, Singapore, 1997, pp. 62–124.
[41] J. Hasegawa, Y. Ozeki, K. Ohkawa, M. Hada, H. Nakatsuji, Theoretical study of the excited states of chlorin, bacteriochlorin, pheophytin a, and chlorophyll a by the SAC/SAC-CI method, J. Phys. Chem. B 102 (1998) 1320–1326.
[42] A. Dreuw, J.L. Weisman, M. Head-Gordon, Long-range charge-transfer excited states in time-dependent density functional theory require non-local exchange, J. Chem. Phys. 119 (2003) 2943–2946.
[43] M.E. Casida, C. Jamorski, K.C. Casida, D.R. Salahub, Molecular excitation energies to high-lying bound states from time-dependent density-functional response theory: characterization and correction of the time-dependent local density approximation ionization threshold, J. Chem. Phys. 108 (1998) 4439–4449.
[44] R. Bauernschmitt, R. Ahlrichs, Calculation of excitation energies within time-dependent density functional theory using auxiliary basis set expansions, Chem. Phys. Lett. 256 (1996) 454–464.
[45] R.B. Stratmann, G.E. Scuseria, M.J. Frisch, An efficient implementation of time dependent density functional theory for the calculation of excitation energies of large molecules, J. Chem. Phys. 109 (1998) 8218–8224.
[46] R.G. Parr, W. Yang, Density-Functional Theory of Atoms and Molecules, Oxford Univ. Press, Oxford, 1989.
[47] D.J. Tozer, R.D. Amos, N.C. Handy, B.O. Roos, L. Serrano-Andres, Does density functional theory contribute to the understanding of excited states of unsaturated organic compounds? Mol. Phys. 97 (1999) 859–868.
[48] L. Bernasconi, M. Sprik, Time dependent density functional theory study of charge-transfer and intramolecular electronic excitations in acetone–water systems, J. Chem. Phys. 119 (2003) 12417–12431.
[49] W.W. Parson, A. Warshel, Spectroscopic properties of photosynthetic reaction centers. 2. Application of the theory to *Rhodopseudomonas viridis*, J. Am. Chem. Soc. 109 (1987) 6152–6163.
[50] M.A. Thompson, M.C. Zerner, A theoretical examination of the electronic structure and spectroscopy of the photosynthetic reaction center from *Rhodopseudomonas viridis*, J. Am. Chem. Soc. 113 (1991) 8210–8215.
[51] J. Hasegawa, K. Ohkawa, H. Nakatsuji, Excited states of the photosynthetic reaction center of *Rhodopseudomonas viridis*: SAC-CI study, J. Phys. Chem. B 102 (1998) 10410–10419.
[52] T. Kobayashi, J-Aggregates, World Scientific, Singapore, 1996.
[53] M.T. Cancès, B. Mennucci, J. Tomasi, A new integral equation formalism for the polarizable continuum model: theoretical background and applications to isotropic and anisotropic dielectrics, J. Chem. Phys. 107 (1997) 3032–3041.
[54] S.E.J. Rigby, J.H.A. Nugent, P.J. O'Malley, ENDOR and special triple resonance studies of chlorophyll cation radicals in photosystem 2, Biochemistry 33 (1994) 10043–10050.
[55] T. Okubo, T. Tomo, M. Sugiura, T. Noguchi, Perturbation of structure of P680 and the charge distribution on its radical cation in isolated reaction center complexes of photosystem ii as revealed by fourier transformation infrared spectroscopy, Biochemistry 46 (2007) 4390–4397.
[56] B.A. Diner, E. Schlodder, P.J. Nixon, W.J. Coleman, F. Rappaport, J. Lavergne, W.F.J. Vermaas, D.A. Chisholm, Site-directed mutants at D1-His198 and D2-His197 of photosystem II in synechocystis PCC 6803: sites of primary charge separation and cation and triplet stabilization, Biochemistry 40 (2001) 9265–9281.
[57] H. Ishikita, W. Saenger, J. Biesiadka, B. Loll, E.-W. Knapp, How photosynthetic reaction centers control oxidation power in chlorophyll pairs P680, P700, and P870, Proc. Natl. Acad. Sci. U. S. A. 103 (2006) 9855–9860.
[58] A.D. McLachlan, Rapid comparison of protein structures, Acta Crystallogr. A38 (1982) 871–873.
[59] W. Humphrey, A. Dalke, K. Schulten, VMD — visual molecular dynamics, J. Mol. Graphics 14 (1996) 33–38.